Coupling of magnetic and optomechanical structuring in cold atoms

T. Ackemann,[1] G. Labeyrie,[2] A. Costa Boquete,[1] G. Baio,[1] J. G. M. Walker,[1] R. Kaiser,[2] G.-L. Oppo,[1] and G. R. M. Robb[1]

[1]*SUPA and Department of Physics, University of Strathclyde, Glasgow G4 0NG, Scotland, United Kingdom*
[2]*Institut de Physique de Nice, Université Côte d'Azur, CNRS, 06560 Valbonne, France*

(Received 21 September 2021; revised 21 April 2022; accepted 17 May 2022; published 8 June 2022)

Self-organized phases in cold atoms as a result of light-mediated interactions can be induced by coupling to internal or external degrees of the atoms. There has been growing interest in the interaction of internal spin degrees of freedom with the optomechanical dynamics of the external center-of-mass motion. We present a model for the coupling between magnetic and optomechanical structuring in a $J = 1/2 \rightarrow J' = 3/2$ system in a single-mirror feedback scheme, which is representative of a larger class of diffractively coupled systems such as longitudinally pumped cavities and counterpropagating-beam schemes. For negative detunings, a linear stability analysis demonstrates that optical pumping and optomechanical driving cooperate to create magnetic ordering. However, for long-period transmission gratings the magnetic driving will strongly dominate the optomechanical driving, unless one operates very close to the existence range of the magnetic instability. At small lattice periods, in particular at wavelength-scale periods, the optomechanical driving will dominate.

DOI: 10.1103/PhysRevA.105.063508

I. INTRODUCTION

Recently, there has been interest in self-organization in cold atoms in transversely pumped cavities [1–11] and via diffractive coupling in longitudinally pumped cavities [12], counterpropagating-beam schemes [13–16], and single-mirror feedback schemes [17–21]. In these schemes coupled light-matter structures are created via optical nonlinearities and the back-action of the structured matter on light. In this paper, we concentrate on single-mirror feedback schemes, but we anticipate that the main conclusions are also valid for other systems. In the single-mirror feedback system (see Fig. 1), effective coupling between atoms is provided by retroreflecting back a laser beam which initially interacted with the atoms. Any spatial structure within the atomic sample will influence the refractive index of the cloud and imprint onto the phase of the transmitted light. Through diffractive dephasing in the feedback loop the retroreflected light will acquire a corresponding structure which will sustain the atomic structure (see [22] for a recent review). The spontaneous formation of atomic density patterns due to optomechanically mediated interaction was demonstrated in [17], where the light-matter interaction was provided via the dipole force. Spontaneous magnetic ordering of dipolar and quadrupolar nature was demonstrated in [19,20,23], where light-matter interaction was mediated by optical pumping. The interplay between optomechanical structures and the electronic two-level nonlinearity was studied in [17,24]. In this contribution, we address the question of whether optomechanical and magnetic orderings can exist together and potentially support each other. This complements recent interest in mixed spin-density textures in cavity QED systems [8,11,25–29].

A simplified $J = 1/2 \rightarrow J' = 3/2$ model for the Rb transition (Fig. 2) allows us to take into account dipolar magnetic structures analogous to spin-1/2 magnets and the optomechanical effects due to light shifts. Figure 3(a) illustrates the magnetization of atoms and the light spin patterns, on the one hand, and the dipole potentials and the resulting bunching, on the other hand. It confirms that for negative detuning the two mechanisms will support each other: Where optical pumping by the optical spin structures leads to the prevalence of, e.g., a population with a positive magnetic quantum number [red solid line and green dotted line in Fig. 3(a) at, e.g., point 0], this state will also have lower energy in the dipole potential (red dotted line at point 0). Hence, one expects that thresholds are lower and that the resulting magnetization peaks are narrower, more "spiky," than those without the bunching effect [Fig. 3(b)]. The latter might have interesting consequences for

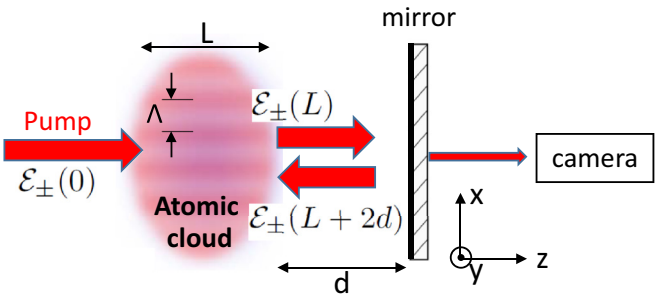

FIG. 1. Experimental scheme for single-mirror feedback. A cloud of length L is driven by a pump laser beam. A plane mirror at a distance d retroreflects the transmitted light back into the cloud. The theoretical treatment assumes $d \gg L$. The optical axis and quantization axis are in the z direction. Structuring is depicted here in the x direction but could, by symmetry, be anywhere in the transverse x-y plane. See text for further explanation.

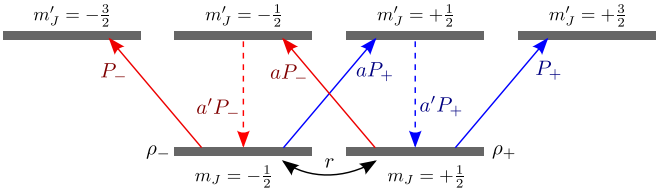

FIG. 2. $J = 1/2 \rightarrow J' = 3/2$ transition. $a = 1/3$ denotes the relative strengths of weak and strong transitions. $a' = 2/9 < a$ allows us to account for a lower optical pumping efficiency as some cycles will return to the original state. The main part of the dynamics takes place in the stretched states with maximum modulus of the magnetic quantum number.

the interaction range of the self-induced lattice, as discussed in [21,22]. Reference [16] discusses the optomechanical part in a $J = 1/2 \rightarrow J' = 3/2$ model following a wave-mixing approach. However, it neglects the intrinsic magnetic instability; that is, it would not lead to an instability for stationary atoms. We will develop a model which can describe both situations in their limiting cases but will use the simplest possible optomechanical model for this assessment, overdamped dynamics in externally imposed molasses, as originally suggested by [13] for diffractively mediated transverse self-organization. The experiments on optomechanical self-organization reported in [17] did not use optical molasses and were interpreted in the framework of a conservative Vlasov-equation model [17,30]. Optical molasses, potentially at lower amplitude and different detuning than that used for the initial trapping, is also interesting for extending the lifetime of the structured state against the heating from scattered pump photons, as demonstrated earlier for the collective atomic recoil lasing instability [31]. The first indications of the extension of the lifetime of structured transverse states were found in counterpropagating beams [16] and single-mirror feedback schemes [32]. Most importantly for our present intentions, the simplicity of the overdamped model compared to the Vlasov model makes it suited to an initial assessment of the interaction between optomechanical and magnetic orderings. As the overdamped and conservative models have the same threshold condition for the same initial temperature [30,33,34], the results developed here for the combined magnetic-overdamped optomechanical model will also provide guidance for the combined magnetic-conservative optomechanical situation. Hence, the current investigations are fruitful even if scattering of molasses photons can be expected to be detrimental to the magnetic ordering because it will provide a background of photons with all polarizations.

II. MODEL

In the experimental scheme (Fig. 1) a cold atomic cloud of ^{87}Rb atoms is driven by a detuned laser beam close to the D_2 line. The transmitted beam is phase modulated by any structure (with transverse spatial period Λ) in the gas which could be due to magnetic ordering of Zeeman substates or a density modulation due to atomic bunching. The beam is retroreflected by a plane mirror of reflectivity R. Diffractive dephasing leads to an amplitude modulation of the backward beam which can then sustain the structure in the cloud. Details

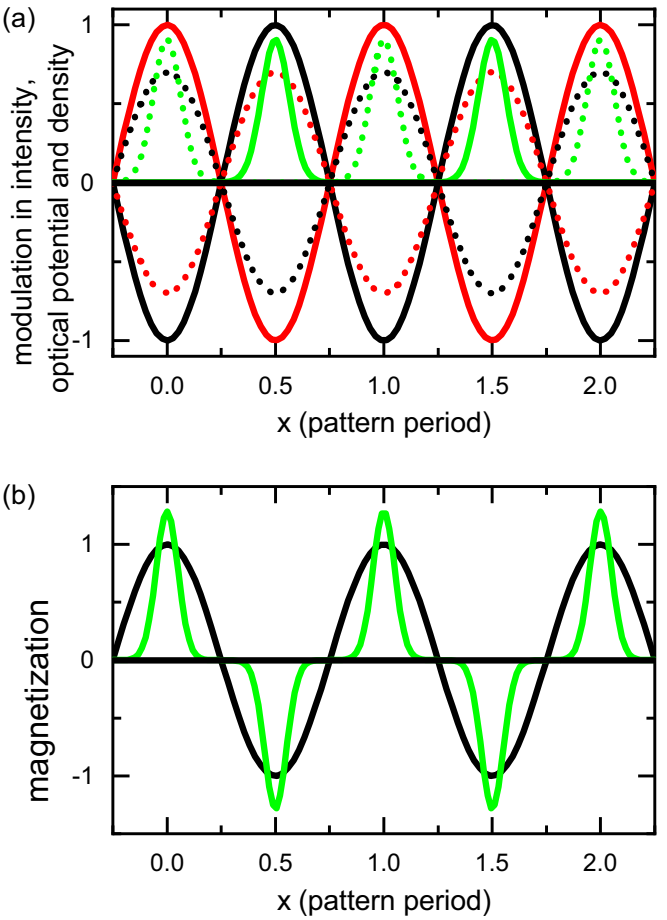

FIG. 3. Schematic illustration of the interplay of magnetic and optomechanical degrees of freedom. The plots depict atomic states and optical fields and potentials in transverse space x measured in units of the lattice period Λ. (a) The intensity of the σ_+ [solid red (dark gray) line] and σ_- (solid black line) components of optical field. Dotted red (dark gray) and black lines are the corresponding potentials for spin-up and spin-down atoms, respectively. The green (light gray) lines indicate the resulting spatially antiphased bunching in density for spin-up (dotted) and spin-down (solid) atoms. The atomic density is narrower than the intensity for cold (enough) atoms. (b) Black line: Atomic magnetization (with dominance of spin-up atoms where positive) resulting from optical pumping from the optical spin patterns [solid red and black lines in (a)] at low saturation. Green (light gray) line: more peaked structure of magnetization if atoms also bunch. The profiles of the curves are artist impressions and are not calculated self-consistently. Here, and in the following, the information in parenthesis indicates gray levels in black and white print version.

can be found in [17,19,20,22]. Self-organization via single-mirror feedback was originally predicted in [35].

For the description of the internal degrees of freedom we follow the spirit of the approach in [36] for a $J = 1/2 \rightarrow J' = 1/2$ transition, adapted to a $J = 1 \rightarrow J' = 2$ transition in [19,20]. In these works, the dynamics for the ground-state magnetization was derived in a semiclassical approximation from the Liouville equation for the density matrix. All excited-state populations, excited-state coherences, and the optical coherence (dipole moment) are adiabatically eliminated as they evolve on the timescale of the lifetime of the

excited state (i.e., <100 ns), whereas the dynamics of the ground state evolves on a timescale of hundreds of microseconds (see [19,20] and below). Afterwards, it is assumed that the total population resides in the ground state. As we are interested in an initial assessment of the interplay of internal (magnetic) and external (optomechanical) degrees of freedom, we consider a further simplification by neglecting excited-state coherences altogether and just consider rate equations for atomic populations (as used in the discussion of Fig. 2). In principle, we could have constructed an even simpler rate-equation model based on a $J = 1/2 \to J' = 1/2$ transition, which would have avoided the complication of multiple pump paths (i.e., $aP_\pm$, $a'P_\pm$) and potential excited-state coherences altogether, but we decided to go for the $J = 1/2 \to J' = 3/2$ transition because it is retains the experimental feature typical of the Rb D_2 line in that the final state of optical pumping is bright and not dark. The model will be valid in the regime where the pump rate is much lower than the decay rate Γ of the excited-state populations and coherences, i.e., saturation values of about a few times 0.01 to about 0.1, depending on the level of qualitative or quantitative accuracy we are interested in.

The optomechanical model is based on overdamped dynamics by means of an additional external optical molasses as used in [13,34]. Under overdamped conditions, the atom density $\rho(\mathbf{r}, t)$ obeys a Smoluchowski drift-diffusion equation [5,37],

$$\partial_t \rho(\mathbf{r},t) = \frac{2\sigma D}{\Gamma} \nabla_\perp \cdot [\rho(\mathbf{r},t)\, \nabla_\perp P(\mathbf{r},t)] + D\nabla_\perp^2 \rho(\mathbf{r},t) \quad (1)$$

$$= \frac{2\sigma D}{\Gamma} [\nabla_\perp \rho \nabla_\perp P + \rho \nabla_\perp^2 P] + D\nabla_\perp^2 \rho(\mathbf{r},t), \quad (2)$$

where D is the cloud diffusivity and $P(\mathbf{r}, t) = \Gamma s/2$ is the pump rate proportional to the total light intensity and the saturation parameter $s(\mathbf{r}, t)$. Δ corresponds to the light-atom detuning in units of the full linewidth Γ. The relative strength of optomechanical driving to thermal fluctuations is characterized by

$$\sigma = \frac{\hbar \Gamma \Delta}{2 k_B T}, \quad (3)$$

where k_B represents the Boltzmann constant and T is the temperature of the cloud. The formulation of Eq. (2) is beneficial as the grad-grad term can be neglected in the linear stability analysis (LSA) because it is second order in spatially inhomogeneous perturbations. It should be noted that $\sigma \sim 1/T$ and $D \sim T$ [see Eq. (29)]; hence, the driving of the optomechanical instability is actually independent of temperature, but the counteracting fluctuations increase with temperature. Because in a dilute thermal gas with well-controlled stray magnetic fields there is no relaxation mechanism for magnetization structures other than the residual atomic motion, this implies that the temperature dependence of the optomechanical and magnetic instabilities will be similar.

The treatment of the magnetization is based on the $J = 1/2 \to J' = 3/2$ transition depicted in Fig. 2. The quantization axis is chosen to be the wave vector of the pump light. Under the assumption that we are interested in rate equations for only the ground-state populations as discussed before, the equations of motions for the populations $\rho_\pm$ of the ground states with $m_j = \pm 1/2$ are

$$\dot{\rho_+} = -\frac{r}{2}(\rho_+ - \rho_-) + a' P_+ \rho_- - a' P_- \rho_+ + D\nabla_\perp^2 \rho_+ + \frac{2\sigma D}{\Gamma}[\nabla_\perp \rho_+ \nabla_\perp (P_+ + aP_-) + \rho_+ \nabla_\perp^2 (P_+ + aP_-)], \quad (4)$$

$$\dot{\rho_-} = -\frac{r}{2}(\rho_- - \rho_+) - a' P_+ \rho_- + a' P_- \rho_+ + D\nabla_\perp^2 \rho_- + \frac{2\sigma D}{\Gamma}[\nabla_\perp \rho_- \nabla_\perp (P_- + aP_+) + \rho_- \nabla_\perp^2 (P_- + aP_+)], \quad (5)$$

with $a = 1/3$ and $a' = 2/9$ [38].

The effective decay rate r for the magnetization due to the residual atomic motion introduced in [19] is

$$r = \frac{4}{\pi \Lambda} \sqrt{\frac{8 k_B T}{\pi M}}. \quad (6)$$

It results from an average time of atoms needing to cross a pattern period ballistically if no velocity damping by molasses is present. It will be dropped in the combined model with diffusive damping by D. However, it is useful to keep for the moment to compare it to the established theory for magnetic self-organization.

The populations are separated into total density ρ and orientation w,

$$\rho = \rho_+ + \rho_-, \quad (7)$$

$$w = \rho_+ - \rho_-, \quad (8)$$

$$\rho_+ = \frac{w + \rho}{2}, \quad (9)$$

$$\rho_- = \frac{-w + \rho}{2}. \quad (10)$$

To make a connection to the two-level optomechanical model, ϕ_S is the linear phase shift if the whole population is in one of the stretched states. Then the linear phase shift for equal population $\rho_+ = \rho_- = 1/2$ is

$$\phi_{\text{lin}} = \frac{1+a}{2} \phi_S = b_0 \frac{\Delta}{\Gamma [1 + (2\Delta/\Gamma)^2]}, \quad (11)$$

where b_0 is the optical density in the line center measured for equal Zeeman populations. This formulation implies the normalization $\rho = 1$ in the homogeneous state. The equations of motion are

$$\dot{w} = -rw + a'(P_+ + -P_-)\rho - a'(P_+ + P_-)w + D\nabla_\perp^2 w + \frac{\sigma D}{\Gamma}[w(1+a)\nabla_\perp^2 (P_+ + P_-) + \rho(1-a)\nabla_\perp^2 (P_+ - P_-)] + \frac{\sigma D}{\Gamma} \nabla_\perp (w+\rho) \cdot \nabla_\perp (P_+ + aP_-) + \frac{\sigma D}{\Gamma} \nabla_\perp (w-\rho) \cdot \nabla_\perp (P_- + aP_+), \quad (12)$$

$$\dot{\rho} = D\nabla_\perp^2\rho + \frac{\sigma D}{\Gamma}\left[\rho(1+a)\nabla_\perp^2(P_+ + P_-) + w(1-a)\nabla_\perp^2(P_+ - P_-)\right] + \frac{\sigma D}{\Gamma}\,\boldsymbol{\nabla}_\perp(w+\rho)\cdot\boldsymbol{\nabla}_\perp(P_+ + aP_-) + \frac{\sigma D}{\Gamma}\,\boldsymbol{\nabla}_\perp(w-\rho)\cdot\boldsymbol{\nabla}_\perp(P_- + aP_+). \tag{13}$$

The transmitted field is given by

$$\mathcal{E}_\pm(L) = \mathcal{E}_\pm(0)\exp\left(i\phi_S\rho_\pm + ia\phi_S\rho_\mp\right) \tag{14}$$

$$= \mathcal{E}_\pm(0)\exp\left(i\phi_{\rm lin}\rho \pm i\phi_{\rm lin}\frac{1-a}{1+a}\,w\right), \tag{15}$$

where $\mathcal{E}_\pm$ refers to the complex field amplitude of the $\sigma_\pm$-polarization components which are scaled such that their squares are the pump rates $P_\pm$. The argument in parentheses refers to the position on the z axis. $\mathcal{E}_\pm(0)$ is the input field at the entrance of the cloud, and $\mathcal{E}_\pm(L)$ is the one at the exit. It is assumed that the atomic variables do not change over z (quasi-two-dimensional situation). It is also assumed that the cloud is diffractively thin; that is, we can neglect diffraction within the medium. The backward field is then obtained in Fourier space. The diffractive dephasing between the on-axis pump and the off-axis spontaneous sidebands of the field is described by the phasor $\Theta = q^2 \times z/(2k) = q^2 \times d/k$ after propagation of a distance $z = 2d$ to the mirror and back [22,35]. The total pump rate is taken to be the sum of the intensities of the forward and backward fields neglecting the interference of the counterpropagating beams and the approximately wavelength-scale gratings created by it. The restriction to a diffractively thin medium and the neglect of wavelength-scale gratings is useful for this discussion of the interaction between optomechanical and optical pumping nonlinearities and is sufficient for a qualitative description of our experimental situation in most circumstances [22]. Extensions are quite complex and are discussed for the simple case of a two-level nonlinearity in [39]. We will comment on the limitations of this approach where appropriate below.

The input field is linearly polarized, $|\mathcal{E}_+(0)|^2 = |\mathcal{E}_-(0)|^2 = P_0$. For a $J = 1/2$ ground state allowing only for dipolar ordering the phase between the $\sigma_\pm$ components is not important for the optical pumping in the ground state. Hence, any transverse input polarization is possible. The spontaneous emergence of π light (polarized parallel to the quantization axis) is not expected and has not been reported in the literature for longitudinal pumping as it would demand coupling via a checkerboard pattern in the longitudinal direction and at least one transverse direction on wavelength scales. This is the natural situation in transversely pumped cavities but not in systems with a single distinguished axis such as the single-mirror feedback system, counterpropagating beams, and longitudinally pumped cavities.

The homogeneous solution for the system is a homogeneous density, $\rho_h = 1$, and zero orientation, $w_h = 0$. The ansatz for the linear stability analysis is then

$$\rho = 1 + \delta\rho, \tag{16}$$

$$w = \delta w, \tag{17}$$

where $\delta\rho$ and δw are small spatially periodic functions, $\sim\cos(\vec{q}\cdot\vec{r})$, with wave vector $\vec{q}$ and position vector $\vec{r}$ in two-dimensional transverse space. As the system is rotational symmetric, the threshold condition does not depend on the direction of $\vec{q}$, only on the wave number $q = |\vec{q}|$ (this was already used in the calculation of the diffractive phasor Θ), and can be obtained by considering a single spatial harmonic. The linear expansion of the transmitted field yields

$$\mathcal{E}_\pm(L) \approx \mathcal{E}_\pm(0)\exp\left(i\phi_{\rm lin}\right) \times (1 + i\phi_{\rm lin}\delta\rho)\left(1 \pm i\phi_{\rm lin}\delta w\frac{1-a}{1+a}\right) \tag{18}$$

$$\approx \mathcal{E}_\pm(0)\exp\left(i\phi_{\rm lin}\right) \times \left(1 + i\phi_{\rm lin}\delta\rho \pm i\phi_{\rm lin}\delta w\frac{1-a}{1+a}\right). \tag{19}$$

This yields

$$\mathcal{E}_\pm(L) = \mathcal{E}_\pm(0)\exp\left(i\phi_{\rm lin}\right)(1 + ie^{i\Theta}\phi_{\rm lin}\delta\rho) \times \left(1 \pm ie^{i\Theta}\phi_{\rm lin}\delta w\frac{1-a}{1+a}\right), \tag{20}$$

$$|\mathcal{E}_\pm(L+2d)|^2 \approx |\mathcal{E}_\pm(0)|^2\left(1 - 2\phi_{\rm lin}\sin\Theta\delta\rho \mp 2\phi_{\rm lin}\sin\Theta\delta w\frac{1-a}{1+a}\right), \tag{21}$$

$$P_\pm(L+2d) = P_0\left(1 - 2\phi_{\rm lin}\sin\Theta\delta\rho \mp 2\phi_{\rm lin}\sin\Theta\delta w\frac{1-a}{1+a}\right), \tag{22}$$

where we assume that the input light is linearly polarized and hence $|\mathcal{E}_+(0)|^2 = |\mathcal{E}_-(0)|^2 = P_0$. Note that the phase of the reentrant $\sigma_\pm$ fields is not affected for a $J = 1/2$ ground state; that is, the polarization direction is not modulated, just the helicity.

A linear stability analysis of the density gives

$$\delta\dot{\rho} = -Dq^2\delta\rho + \frac{4\sigma D\phi_{\rm lin}\sin\Theta P_0 R q^2}{\Gamma}(1+a)\,\delta\rho, \tag{23}$$

with threshold

$$P_{0,\rm th} = \frac{\Gamma}{4\phi_{\rm lin}\sin\Theta\sigma R(1+a)}. \tag{24}$$

Note that for linearly polarized light $P_{0,\rm th}$ represents only half the input intensity. This result agrees with the expression for the scalar case in [34] for $a = 0$. The minimal threshold is achieved for $\sin\Theta = 1$, which corresponds to a phase shift of $\pi/2$ after a quarter of the Talbot distance. This provides positive feedback for a self-focusing situation [17,22,35]. Note that this is independent of the sign of detuning as both σ and $\phi_{\rm lin}$ change sign with detuning. The threshold condition for the overdamped case is the same as that for the conservative case at the same initial temperature. Equation (6) of [30] reduces to Eq. (24) for high enough optical densities. At these optical

densities (and the one considered below) the optical dipole potential can be taken to be proportional to $\log(1+P) \approx P$. Using $\ln(1+P)$ as the expression for the dipole potential in the derivation here would lead to Eq. (6) of [30].

The LSA for the orientation gives

$$\begin{aligned}\delta\dot{w} = &-r\delta w - Dq^2\delta w - 2a'P_0(1+R)\delta w \\ &- 4RP_0\phi_{\rm lin}\sin\Theta a'\frac{1-a}{1+a}\,\delta w \\ &+ \frac{4\sigma D\phi_{\rm lin}\sin\Theta P_0 Rq^2}{\Gamma}\,\frac{(1-a)^2}{1+a}\,\delta w, \end{aligned} \tag{25}$$

where the first line describes decay and saturation by the total pump rate, the second line describes driving by optical pumping, and the last line describes driving by optomechanics. The magnetic decay and driving terms have the same structure as derived in [19] for a $J = 1 \to J' = 2$ transition but with different numerical values for the prefactors. The term describing optomechanical driving of a magnetic state in the last line is the one derived in this treatment. For negative detuning ($\Delta < 0$, $\sigma < 0$, $\phi_{\rm lin} < 0$), the minimal threshold is reached for $\sin\Theta = 1$, and the optomechanical effect enhances the magnetic instability as expected from the considerations in Fig. 3. For positive detuning, the optimal feedback is obtained for the magnetic instability for $\sin\Theta = -1$ and for the optomechanical instability for $\sin\Theta = 1$; that is, the two instabilities oppose each other. This is because the magnetic one is self-defocusing (as the trapping state is bright on the D_2 line, the optical pumping nonlinearity is defocusing for blue detuning) and the optomechanical one is focusing. In the potential picture in Fig. 3, for blue detuning the optically pumped atoms would be expelled from the intensity maxima optimally sustaining the magnetic ordering. The threshold is given by

$$P_{0,\rm th} = \frac{Dq^2}{-2a'(1+R) - 4R\phi_{\rm lin}\sin\Theta a'\frac{1-a}{1+a} + 4R\phi_{\rm lin}\sin\Theta q^2\frac{\sigma D}{\Gamma}\frac{(1-a)^2}{1+a}}. \tag{26}$$

An interesting aspect is that the two instabilities are not directly coupled in linear order as the equations for $\delta\rho$ and δw are not coupled to each other. The reason seems to be that a magnetic instability at q would drive a density modulation at $2q$. A density modulation at q will drive a magnetic modulation at $q/2$. These are second-order processes.

III. ANALYSIS

In a first step, Fig. 4 compares the relaxation of the structures assuming ballistic motion using an effective decay rate r, Eq. (6), with the diffusive ansatz with molasses (giving a decay rate of Dq^2) for the magnetic self-ordering. Obviously, in both cases relaxation decreases with increasing lattice period Λ, but the functional relationship is proportional to q^{-1} for the ballistic case and q^{-2} for the diffusive one. Matching the rates for the experiment performed at Institut de Physique de Nice (INPYNI) using a large atomic cloud [17,20] at the relevant scale of about $\Lambda \approx 100\,\mu$m gives a diffusion coefficient of about (7–9) $\times 10^{-7}$m^2/s. For the experiment performed at Strathclyde with a smaller cloud [19], it is $D \approx 3 \times 10^{-7}$m^2/s to match at $\Lambda \approx 50\,\mu$m. These values are compatible with diffusion coefficients obtained in optical

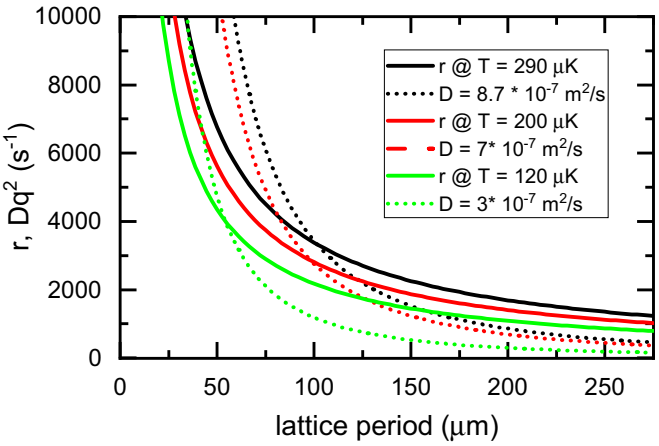

FIG. 4. Effective relaxation rate (solid lines) vs lattice period from Eq. (6) for the temperatures relevant for [17,19,20] compared to diffusive modeling (dotted lines) for different diffusion constants. Black (corresponding to the situation in [17]): solid line, $T = 290\ \mu$K; dotted line, 8.7×10^{-7}m^2/s. Red (dark gray; corresponding to the situation in [20]): solid line, $T = 200\ \mu$K; dotted line, 7×10^{-7}m^2/s. Green (light gray; corresponding to the situation in [19]): solid line, $T = 120\ \mu$K, dotted line, 3×10^{-7}m^2/s.

molasses. Measurements in a lin-perp-lin configuration in [40] indicate values of $D \approx$ (1–2) $\times 10^{-7}$m^2/s for the diffusion coefficient above saturation intensity and (2–3) $\times 10^{-7}$m^2/s at lower intensities. This order of magnitude is fine for the current preliminary estimations. Properties of the molasses would need to be optimized anyway.

Temperature and the diffusion coefficient are not independent in an optical molasses. Temperature is related to the momentum diffusion coefficient D_p and the velocity damping coefficient α [40,41] by

$$T = \frac{D_p}{\alpha k_b}, \tag{27}$$

and the space diffusion coefficient is given by

$$D = \frac{D_p}{\alpha^2}. \tag{28}$$

Hence,

$$D = \frac{k_B T}{\alpha}. \tag{29}$$

For the velocity-damping coefficient we use the estimation of [40] for a three-dimensional (3D) lin-perp-lin molasses,

$$\alpha \approx \tfrac{3}{7}\hbar k^2\,|\Delta_M|, \tag{30}$$

where Δ_M denotes the detuning of the molasses normalized to Γ. Detunings in the range of 1.35–1.9 will then produce the combination of temperatures and diffusion coefficients identified in Fig. 4, and taking $|\Delta_M| = 1.8$ will sweep the diffusion coefficient from 3.1×10^{-7}m^2/s at 120 μK to 7.6×10^{-7}m^2/s at 290 μK; that is, it allows us to cover the range of estimations intended here.

Figure 5(a) shows the threshold saturation parameter, $s_0 = P_0/(\Gamma/2)$, for one circular component of the linearly polarized

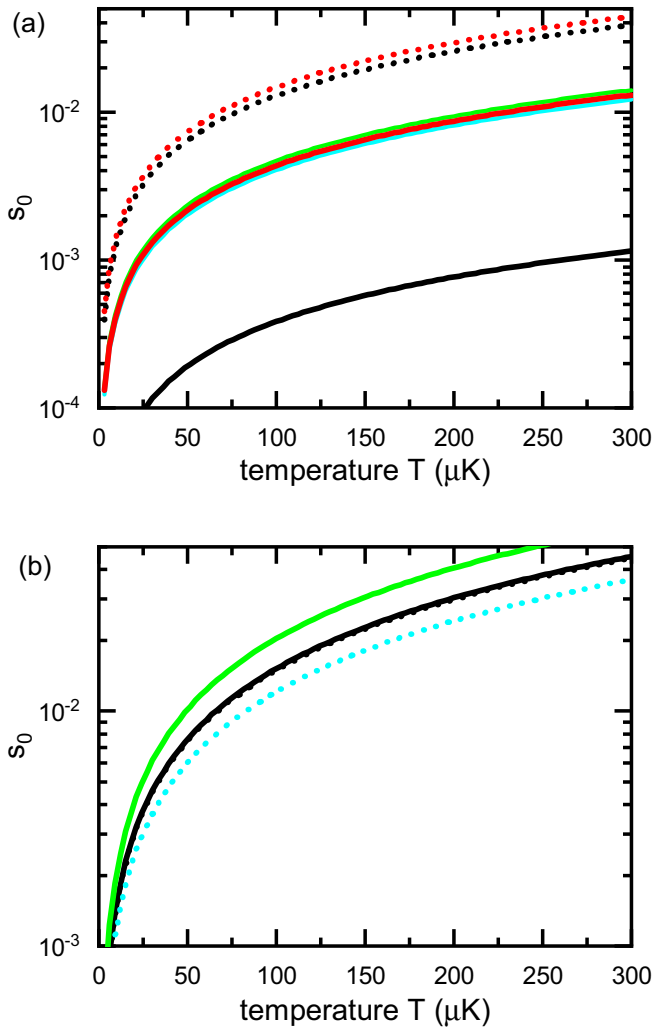

FIG. 5. Threshold saturation parameter for one circular component vs temperature for $\Delta = -8.6$, $\Lambda = 100$ μm. (a) Black lines ($b_0 = 80$): solid line, threshold for magnetic ordering; dotted line, threshold for optomechanical bunching. The thresholds for combined magnetic and optomechanical driving of magnetic ordering are essentially indistinguishable from the black solid line for magnetic ordering alone at this scale. Red (dark gray) lines ($b_0 = 70$): solid line, threshold for magnetic ordering; dotted line, threshold for optomechanical bunching (both are above their black counterparts). The cyan (light gray) solid line [just below the red (dark gray) solid line] represents the combined threshold for magnetic and optomechanical driving for negative detuning and $b_0 = 70$; the green (light gray) solid line [just above the red (dark gray) solid line] represents positive detuning. (b) Same as (a), but for $b_0 = 69.31$. The cyan line is now dotted to indicate the difference from the green line. The parameter σ changes from infinity at $T = 0$ to 4.3 at $T = 300$ μK via 12.5 at $T = 100$ μK and 8.4 $T = 150$ μK.

input vs temperature for the parameters analyzed in [19,20], $\Delta = -8.6$, $\Lambda = 100\,\mu$m, $b_0 = 80$. The solid black line indicates the threshold for magnetic ordering, Eq. (26); the dotted black line indicates the one for optomechanical bunching, Eq. (24). They are almost two orders of magnitude apart. Indeed, the structures observed in [19,20] were identified as arising from magnetic ordering. The predicted intensity thresholds rise from about 0.2 mW/cm^2 at 100 μK via 0.4 mW/cm^2 at 200 μK to 0.6 mW/cm^2 at 300 μK. The experimentally observed threshold for 200 μK is about 2 mW/cm^2. The difference is attributed to stray magnetic fields, the finite reflectivity of the mirror, and imperfect antireflection coatings of cell windows. The predicted intensity thresholds for the optomechanical bunching rise from about 6.4 mW/cm^2 at 100 μK via 13 mW/cm^2 at 200 μK to 19 mW/cm^2 at 300 μK. No experiments on optomechanics have been performed in this parameter range, but the experiments in [17] can serve as a guideline as the threshold should be independent of detuning and dependent on only the initial temperature at the optical densities used, independent of whether the molasses is present or not [30,33,34]. The minimum thresholds found there are about 50 mW/cm^2 at 290 μK, i.e., in reasonable agreement with the estimation allowing for some heating effects by the pump beams.

As the magnetic and optomechanical thresholds are quite different, the thresholds for combined optical pumping–optomechanical driving of the magnetic ordering are essentially indistinguishable from the optical pumping one for both detunings and are not included in Fig. 5(a) for $b_0 = 80$. The reason that temperature is not a strongly distinguishing parameter between instabilities is that, as indicated before, the driving is independent of temperature for both instabilities (σD is independent of temperature) but both are counteracted by the residual atomic motion. By introducing a transverse magnetic field one can open a relaxation channel for the orientation and destroy it (e.g., [19]), leaving the possibility of optomechanical and/or electronic structuring. However, no detailed experimental investigations of the transition have been done.

This changes somewhat at lower optical densities as the presence of the saturation term in the expression for the magnetic ordering implies a minimum value of the linear phase shift, $\phi_{\rm lin} > (1 + R)/R$. For $\Delta = -8.6$ this implies $b_0 > 69.3$. The solid and dotted red (dark gray) lines in Fig. 5(a) denote the situation for $b_0 = 70$. Both the optomechanical and magnetic thresholds increased, but the gap between them narrowed as the magnetic threshold is much more susceptible to a density change due to the saturation term. In this situation the thresholds for combined driving are discernible from the optical pumping one, leading to a reduction of the threshold for negative detuning [cyan (light gray) line] and an increase of the threshold for positive detuning [green (light gray) line]. Going closer to the magnetic threshold, $b_0 = 69.31$, the optomechanical and magnetic thresholds nearly coincide [Fig. 5(b)]. The cooperation between the optomechanical and magnetic drivings leads now to a substantial reduction of the threshold [dotted cyan (light gray) line] for negative detuning, whereas the combined threshold is enhanced for positive detuning [green (light gray) line], demonstrating the interaction between the driving terms. Experiments in the apparatus at Strathclyde are performed at lower optical density, measured to be $b_0 \approx 27$, which is very close to the minimum density required [19,22]. More robust agreement between experiment and theory has been obtained assuming $b_0 \approx 30$ [23]. The current considerations indicate that the self-organization might have been helped by the reinforcement between

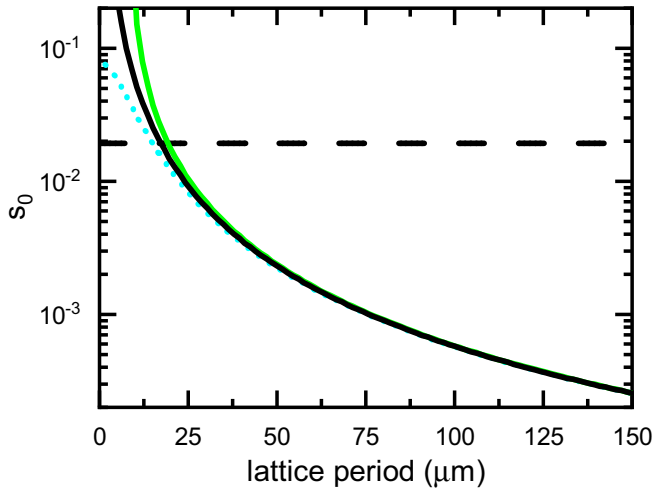

FIG. 6. Threshold saturation parameter for one circular component vs lattice period for $\Delta = -8.6$, $b_0 = 80$, $T = 150\,\mu$K. Solid black line, threshold for magnetic ordering; dashed black line, threshold for optomechanical bunching; cyan (light gray) dotted line, combined threshold for magnetic and optomechanical driving of magnetic ordering for negative detuning; and green (light gray) solid line, combined threshold for positive detuning $\Delta = +8.6$.

optomechanical and magnetic degrees of freedom already under this situation. (There is no quantitative correspondence between thresholds quoted here and in [19,22] because the latter papers assume a more realistic $J = 1 \rightarrow J' = 2$ transition which changes the pre-factors of order 1 in the susceptibilities and pump rates.) One can also note that there is a strong preference for magnetic patterns to appear for negative detuning [19,20,22] and only some indications are found for positive detuning [42]. Although this observation agrees in tendency with the prediction above, the main reason for this asymmetry is probably the fact that under self-defocusing conditions (as indicated, the optical pumping nonlinearity behaves self-defocusing for positive detuning on the D_2 line) the assumption of a homogeneous distribution of orientation along the beam axis is not well justified, as previously identified for defocusing situations [17,22,43].

However, one difference between the magnetic and optomechanical self-organizations is that in the latter not only relaxation but also driving increases with increasing transverse wave number, i.e., decreasing lattice period, as the dipole force depends on the gradient of the optical potential. Hence, these effects cancel, and the threshold is independent of wave number, as is apparent from Eq. (24). The same holds for the conservative model discussed in [18]. In reality we expect stochastic effects due to the scattering of pump photons to favor longer-period grating over shorter-period ones, in particular for the conservative case, as argued in [17]. We will discuss some aspects of this further below. Figure 6 shows an analysis of a representative temperature around the Doppler temperature, $T = 150\,\mu$K. The horizontal dashed line indicates the optomechanical threshold for density bunching that is independent of lattice period in the framework of this treatment. The magnetic threshold increases with decreasing lattice period (solid black line) as the structure is washed out by the residual transverse atomic motion. The intersection is at $\Lambda \approx 17\,\mu$m. For smaller lattice periods the density modulation is the primary driver. In the vicinity of this point, there is again the splitting of the threshold condition for the magnetic case, which is apparent because the optomechanical driving either supports (dotted cyan line, $\Delta < 0$) or inhibits (solid green line, $\Delta > 0$) the magnetic ordering. It should be noted that this point is not accessible in an experiment with thermal atoms as the small transverse period violates the assumption of a diffractively thin medium. The minimum length scale which can be obtained is of the order of $\Lambda_{\min} \approx \sqrt{\lambda L}$, where L is the longitudinal extension of the cloud [22,39]. This scale agrees roughly with the scale expected for an instability in two independent counterpropagating pump beams [44,45]. This implies $L_{\max} \approx 0.37$ mm, which is much smaller than needed for thermal clouds with sufficient optical density to reach the threshold ($L \approx 2$–10 mm in our experiments). The region in question also gives a relatively high threshold of $s \approx 0.1$ where the limitation to ground-state dynamics becomes questionable. Hence, to stay within the assumptions of the ground-state model, the temperature of the cloud needs to be lower, and/or the optical density needs to be higher, demanding further optimization of the trapping and cooling processes. However, these considerations can be important for extending the treatment in [18,21] on optomechanical self-organization in quantum degenerate gases with optical feedback to spinor Bose-Einstein condensates because they have sufficient optical density in small clouds.

This limitation on period holds for gratings stemming from the interference between a pump beam and (nearly) copropagating sidebands (so-called transmission gratings). Interference between a pump and (nearly) counterpropagating sidebands results in gratings with a wave number slightly smaller than $2k$ (so-called reflection gratings). Although not directly included in our analysis, the argument can be made that these gratings are mainly driven by optomechanical effects. This was, indeed, argued in [14–16], which treat optomechanical bunching concentrating on reflection gratings in a $J = 1/2 \rightarrow J' = 3/2$ transition without considering the option of a purely magnetic ordering.

A final consideration is that the presence of the 3D molasses implies a background field with many polarization components, which can be expected to scramble the magnetic substates and to counteract the optical pumping by the pump beams. Formally, this can be seen from Eq. (25), in which the intensity-dependent damping term in the first row represents the action of the total pump rate. We model the action of the molasses by adding a corresponding damping $-6P_m$, where P_m is the pump rate of a single molasses beam and no allowance is made for the difference in Clebsch-Gordon coefficients between substates. We also take temperature and diffusion constant to be constant for simplicity. Figure 7 illustrates that a saturation parameter slightly larger than 10^{-3} is already sufficient to drive the magnetic threshold above the optomechanical one. At this point, the total saturation by the pump and molasses which needs to be overcome by the driving is of the order of the optomechanical threshold. Hence, experiments on magnetic ordering will need to be performed without molasses, as in [19,20,23].

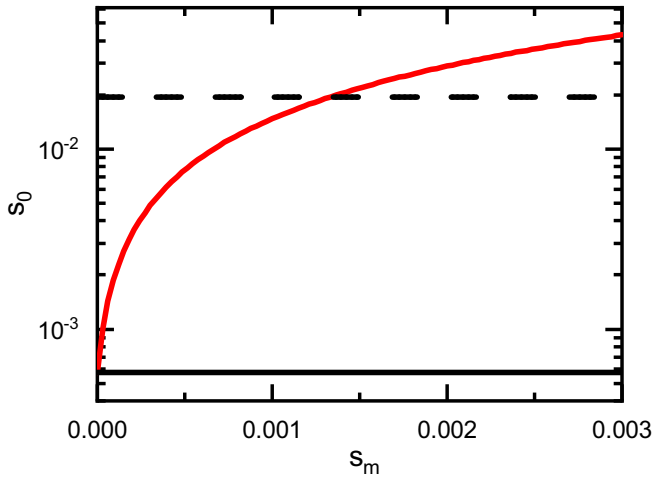

FIG. 7. Threshold saturation parameter for one circular component vs the saturation parameter for one molasses beam for $\Delta = -8.6$, $b_0 = 80$, $T = 150\,\mu$K, $\Lambda = 100\,\mu$m. Horizontal solid black line, threshold for magnetic ordering without molasses; horizontal dashed black line, threshold for optomechanical bunching; red (dark gray) line, the threshold for magnetic ordering including the repumping of the molasses.

IV. CONCLUSIONS

We demonstrated using linear stability analysis that optical pumping and optomechanical driving will cooperate in magnetic ordering for negative detuning, in principle. However, for long-period transmission gratings the driving by optical pumping will strongly dominate. Close to the existence limit of magnetically ordered states (i.e., at low optical density), the additional driving by optomechanics is more important and will help to sustain these states over a larger parameter regime. The background photons from the molasses will scramble the magnetic ordering at quite low saturation values. Hence, an overdamped system with molasses is not attractive for these investigations, and magnetic-optomechanical coupling should be realized without molasses in the conservative limit, with a view of including the potential cooling and heating effects of the pump and self-organized gratings in the long term. Reference [15] found indications for 3D Sisyphus also in the transverse direction after self-organization occurred in a counterpropagating-beam scheme. However, as the optomechanical threshold conditions are identical for the overdamped and conservative cases for the same initial temperature, we expect that the results obtained here with molasses are indicative of what to expect in the conservative case. The current characteristic to establish that the structures are of magnetic origin is their sensitivity to an external transverse magnetic field [19,20]. As for well-controlled magnetic fields, the residual atomic motion represents the fluctuations counteracting both instabilities; temperature cannot be used to favor optomechanical ordering vs magnetic ordering. The prevalence of magnetic structures to enable optomechanical ordering has been broken by introducing a polarizer in the feedback loop to enforce the incident linear polarization state [17]. Switching between circular and linear input polarization is an alternative way to distinguish between magnetic (or mixed) self-organization and optomechanical self-organization without putting a polarizer in the feedback loop and, as such, keeping all residual losses and alignments the same if analyzing the predicted difference between magnetic and optomechanical thresholds. In the analysis, $\phi_{\rm lin}$ needs to be replaced by ϕ_S, and the saturation parameter needs to be low enough to avoid excitation of the excited state. This has a parallel in the experiment of Ref. [8], in which a change in polarization state (there, polarization direction) of the pump also leads to a preference for the density-modulated state over the spin-modulated state. In systems in which the spinor interaction is not implemented via the tensor susceptibility of a transition but by engineered Raman transitions between pseudospins (e.g., [3,6,25,28]), there is still an interesting parallel as the threshold of the superradiance combining spin and recoil effects will depend on the difference between recoil frequency and Raman detuning, i.e., the change with sign of detuning [28].

Reducing the structure period increases the relative importance of the optomechanical driving, and at periods below about 20 μm the optomechanical density structuring will prevail as not only relaxation but also the driving by the dipole force increases. This transition might be observable using quantum degenerate gases which have the necessary optical density in small-size clouds. The results also indicate that optical-pumping-induced wavelength-scale reflection gratings are not significant compared to the long-period transmission gratings. This supports the assumption in [14–16] to treat only optomechanical effects in a counterpropagating-beam scheme. In conclusion, the best prospects for studying the interaction between optomechanical and magnetic drivings for thermal atoms is to use cold and small clouds with structure periods on the order of some tens of micrometers.

Having established the effects of magneto-optomechanical coupling on threshold conditions, it would now be interesting to look at the nonlinear stage of evolution using numerical simulations. Even if the instabilities for density and orientation decouple in linear approximation during the initial stage of the instability, this will not be the case in the saturation regime where the structures achieve significant amplitudes. Modulations of total density will appear even if the instability is driven by the orientation and vice versa. One can expect a narrowing of structures for negative detuning [Fig. 3(b)]. Via the higher harmonics involved, this will have consequences for the coupling behavior across the self-induced lattice [21,22].

ACKNOWLEDGMENTS

The work was supported by the European Training Network ColOpt funded by the European Union Horizon 2020 programme under the Marie Sklodowska-Curie action, Grant Agreement No. 721465. The collaboration between the two groups is further supported by the CNRS-funded Laboratoire International Associ (LIA) “Solace” and the Global Engagement Fund of the University of Strathclyde.

[1] P. Domokos and H. Ritsch, Phys. Rev. Lett. **89**, 253003 (2002).
[2] A. T. Black, H. W. Chan, and V. Vuletic, Phys. Rev. Lett. **91**, 203001 (2003).
[3] F. Dimer, B. Estienne, A. S. Parkins, and H. J. Carmichael, Phys. Rev. A **75**, 013804 (2007).
[4] K. Baumann, C. Guerlin, F. Brennecke, and T. Esslinger, Nature (London) **464**, 1301 (2010).
[5] H. Ritsch, P. Domokos, F. Brennecke, and T. Esslinger, Rev. Mod. Phys. **85**, 553 (2013).
[6] Z. Zhiqiang, C. Lee, R. Kumar, K. J. Arnold, S. J. Masson, A. S. Parkins, and M. Barrett, Optica **4**, 424 (2017).
[7] A. J. Kollar, A. T. Papageorge, V. D. Vaidya, Y. Guo, J. Keeling, and B. L. Lev, Nat. Commun. **8**, 14386 (2017).
[8] M. Landini, N. Dogra, K. Kroeger, L. Hruby, T. Donner, and T. Esslinger, Phys. Rev. Lett. **120**, 223602 (2018).
[9] Y. Guo, R. M. Kroeze, B. P. Marsh, S. Gopalakrishnan, J. Keeling, and B. L. Lev, Nature (London) **599**, 211 (2021).
[10] P. Kirton, M. M. Roses, J. Keeling, and E. G. Dalla Torre, Adv. Quantum Technol. **2**, 1800043 (2019).
[11] F. Mivehvar, F. Piazza, T. Donner, and H. Ritsch, Adv. Phys. **70**, 1 (2021).
[12] E. Tesio, G. R. M. Robb, T. Ackemann, W. J. Firth, and G.-L. Oppo, Phys. Rev. A **86**, 031801(R) (2012).
[13] G. A. Muradyan, Y. Wang, W. Williams, and M. Saffman, in *Nonlinear Guided Waves and Their Applications* (Optical Society of America, Washington, DC, 2005), ThB29.
[14] J. A. Greenberg, B. L. Schmittberger, and D. Gauthier, Opt. Express **19**, 22535 (2011).
[15] B. L. Schmittberger and D. J. Gauthier, New J. Phys. **18**, 103021 (2016).
[16] B. L. Schmittberger and D. J. Gauthier, J. Opt. Soc. Am. B **33**, 1543 (2016).
[17] G. Labeyrie, E. Tesio, P. M. Gomes, G.-L. Oppo, W. J. Firth, G. R. Robb, A. S. Arnold, R. Kaiser, and T. Ackemann, Nat. Photonics **8**, 321 (2014).
[18] G. R. M. Robb, E. Tesio, G.-L. Oppo, W. J. Firth, T. Ackemann, and R. Bonifacio, Phys. Rev. Lett. **114**, 173903 (2015).
[19] I. Krešić, G. Labeyrie, G. R. M. Robb, G.-L. Oppo, P. M. Gomes, P. Griffin, R. Kaiser, and T. Ackemann, Commun. Phys. **1**, 33 (2018).
[20] G. Labeyrie, I. Krešić, G. R. M. Robb, G.-L. Oppo, R. Kaiser, and T. Ackemann, Optica **5**, 1322 (2018).
[21] Y.-C. Zhang, V. Walther, and T. Pohl, Phys. Rev. Lett. **121**, 073604 (2018).
[22] T. Ackemann, G. Labeyrie, G. Baio, I. Krešić, J. G. M. Walker, A. Costa Boquete, P. Griffin, W. J. Firth, R. Kaiser, G.-L. Oppo, G. R. M. Robb, Atoms **9**, 35 (2021).
[23] I. Krešić, G. R. M. Robb, G. Labeyrie, R. Kaiser, and T. Ackemann, Phys. Rev. A **99**, 053851 (2019).
[24] A. Camara, R. Kaiser, G. Labeyrie, W. J. Firth, G.-L. Oppo, G. R. M. Robb, A. S. Arnold, and T. Ackemann, Phys. Rev. A **92**, 013820 (2015).
[25] F. Mivehvar, F. Piazza, and H. Ritsch, Phys. Rev. Lett. **119**, 063602 (2017).
[26] S. B. Jäger, M. Xu, S. Schütz, M. J. Holland, and G. Morigi, Phys. Rev. A **95**, 063852 (2017).
[27] J. Kohler, J. A. Gerber, E. Dowd, and D. M. Stamper-Kurn, Phys. Rev. Lett. **120**, 013601 (2018).
[28] R. M. Kroeze, Y. Guo, V. D. Vaidya, J. Keeling, and B. L. Lev, Phys. Rev. Lett. **121**, 163601 (2018).
[29] N. Masalaeva, W. Niedenzu, F. Mivehvar, and H. Ritsch, Phys. Rev. Research **3**, 013173 (2021).
[30] E. Tesio, G. R. M. Robb, T. Ackemann, W. J. Firth, and G.-L. Oppo, Phys. Rev. Lett. **112**, 043901 (2014).
[31] C. von Cube, S. Slama, D. Kruse, C. Zimmermann, P. W. Courteille, G. R. M. Robb, N. Piovella, and R. Bonifacio, Phys. Rev. Lett. **93**, 083601 (2004).
[32] P. M. Gomes, I. Krešić, and T. Ackemann (unpublished).
[33] E. Tesio, Ph.D. thesis, University of Strathclyde, 2014.
[34] G. Baio, G. R. M. Robb, A. M. Yao, G.-L. Oppo, and T. Ackemann, Phys. Rev. Lett. **126**, 203201 (2021).
[35] W. J. Firth, J. Mod. Opt. **37**, 151 (1990).
[36] F. Mitschke, R. Deserno, W. Lange, and J. Mlynek, Phys. Rev. A **33**, 3219 (1986).
[37] K. M. O'Hara, S. R. Granade, M. E. Gehm, and J. E. Thomas, Phys. Rev. A **63**, 043403 (2001).
[38] J. Dalibard and C. Cohen-Tannoudji, J. Opt. Soc. Am. B **6**, 2023 (1989).
[39] W. J. Firth, I. Krešić, G. Labeyrie, A. Camara, and T. Ackemann, Phys. Rev. A **96**, 053806 (2017).
[40] T. W. Hodapp, C. Gerz, C. Furtlehner, C. I. Westbrook, W. D. Phillips, and J. Dalibard, Appl. Phys. B **60**, 135 (1995).
[41] P. D. Lett, W. D. Phillips, S. L. Rolston, C. E. Tanner, R. N. Watts, and C. I. Westbrook, J. Opt. Soc. Am. B **6**, 2084 (1989).
[42] G. Labeyrie (unpublished).
[43] A. Aumann, T. Ackemann, E. Große Westhoff, and W. Lange, Phys. Rev. E **66**, 046220 (2002).
[44] W. J. Firth, A. Fitzgerald, and C. Pare, J. Opt. Soc. Am. B **7**, 1087 (1990).
[45] W. J. Firth and C. Pare, Opt. Lett. **13**, 1096 (1990).